BIOMICROFLUIDICS **4**, 043001 (2010)

Review Article: Recent advancements in optofluidic flow cytometer

Sung Hwan Cho,[1,a)] Jessica M. Godin,[2] Chun-Hao Chen,[3] Wen Qiao,[2]
Hosuk Lee,[2] and Yu-Hwa Lo[1,2]
[1]*Materials Science and Engineering Program, University of California San Diego,*
La Jolla, California 92093-0418, USA
[2]*Department of Electrical and Computer Engineering, University of California San Diego,*
La Jolla, California 92093-0407, USA
[3]*Department of Bioengineering, University of California San Diego, La Jolla, California*
92093-0412, USA

(Received 16 August 2010; accepted 14 October 2010; published online 30 December 2010)

There is an increasing need to develop optofluidic flow cytometers. Optofluidics, where optics and microfluidics work together to create novel functionalities on a small chip, holds great promise for lab-on-a-chip flow cytometry. The development of a low-cost, compact, handheld flow cytometer and microfluorescence-activated cell sorter system could have a significant impact on the field of point-of-care diagnostics, improving health care in, for example, underserved areas of Africa and Asia, that struggle with epidemics such as HIV/AIDS. In this paper, we review recent advancements in microfluidics, on-chip optics, novel detection architectures, and integrated sorting mechanisms. © *2010 American Institute of Physics.* [doi:10.1063/1.3511706]

I. INTRODUCTION

A. Flow cytometry—principles and applications in biomedical research

The flow cytometer and the fluorescence-activated cell sorter (FACS) are widely used analysis tools in biomedical research and clinical diagnostics. These tools greatly facilitate the study of both physical properties (e.g., size, shape) and biochemical properties (e.g., cell cycle distribution, DNA contents) of biological samples such as cells. Information about the cells of interest is obtained optically in a nondestructive and quantitative manner.[1,2] Flow cytometry is commonly used in a variety of biomedical fields (for example, immunology or cellular and molecular biology), allowing studies of cell cycle analysis, gene expression levels, intracellular cytokine measurement, vaccine analysis, phagocytosis, and much more.[3–6] Besides its applications in basic biomedical research, flow cytometry has become an important clinical tool to monitor the progression of hematological diseases such as leukemia and AIDS.[2,7] A state-of-the-art FACS system can optically screen tens of thousands of cells per second and then sort out a specific subpopulation of cells for further analysis, enabling studies of rare samples, such as stem cells.[8]

Traditional flow cytometry detects and analyzes optical signals (angular light scatter or emitted fluorescence) to identify individual cells or biological samples. Figure 1 illustrates a simple four-parameter (e.g., two scattering and two fluorescent signals) flow cytometer. The suspended cells are introduced to the fluidic system and hydrodynamically focused by a sheath flow, ensuring that cells travel through the center of the fluidic channel at a uniform velocity. Upon arrival at the interrogation zone, the cells are each individually optically interrogated by a focused laser beam (typically ~20–40 μm width) passing perpendicularly across the channel, as shown in Fig. 1. The optical detection system, which consists of lenses, mirrors, filters, and photodetectors, collects the detection signals. Forward light scatter (FSC), orthogonal (side) light scatter (SSC), and

---

[a)] Author to whom correspondence should be addressed. Electronic mail: scho@logroup.ucsd.edu.

© 2010 American Institute of Physics

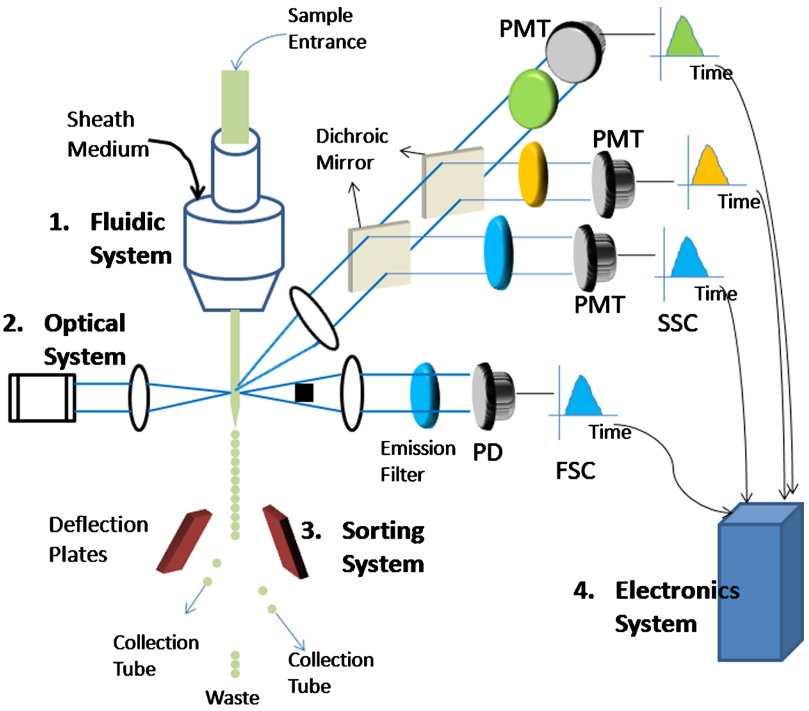

FIG. 1. Schematic of a FACS system that can detect two scattered and two fluorescent light signals. It consists of (1) a fluidic system, (2) an optical system (illumination and detection), (3) a sorting system, and (4) an electronic control system (Ref. 9).

several fluorescence bands (FL1, FL2, etc.) are simultaneously obtained as each cell passes by the laser beam. The FSC line (~1°–10° from the laser axis) intensity yields information related to particle size and refractive index. The light intensity measured by the SSC line (located at about 90° from the optical axis) generally relates to the degree of internal structure (granularity) of the cell. In addition to these two scatter collection lines, a simple flow cytometer might include 3–4 fluorescence channels (whereas more high-end instruments might be able to discriminate up to 17 colors or even more in addition to two scattering light collection).[10,11] The quality of both the optical and fluidic systems is critical for device performance and reliability. The cells must pass through a small, uniform, stable illumination beam at a consistent location, and light scatter and fluorescence measurements must be obtained from a single cell only (no coincidence events) and be free from excess noise (stray light, scatter from debris, etc). Photodetectors, either photodiodes or photomultiplier tubes (PMTs), collect the optical signals. For fluorescence, dichroic mirrors split the emission spectrum to route the desired bands to the appropriate PMT, while optical filters further define the wavelength band passed to each detector. The measured signal intensities for each parameter are used to distinguish between various sample subpopulations (e.g., light scatter can distinguish monocytes, lymphocytes, and granulocytes in a leukocyte sample, while fluorescence can further distinguish cells by surface antigens, such as CD4+ or CD8+ lymphocytes).

After identification by the optical system, a downstream sorting system can isolate cells of interest. This is typically performed via a droplet-based approach. As cells approach the sorting chamber, vibrations break the main fluid stream into charged droplets, allowing their paths to be manipulated by a pair of electrically charged deflection plates. Through a feedback control system (e.g., the decision making process after the cell is detected and identified upstream), the polarity of the plates changes in order to deflect cells of interest into the proper collection tubes for postprocessing analysis.

There are various sources to learn, in great depth, the principles of flow cytometry and its applications in biomedical or clinical research.[1,2] In addition, several comprehensive reviews of chip-based cytometry also exist.[9,12,13] Thus, this review article will focus on recent advances in developing a miniaturized, microfluidic flow cytometer, where optics and microfluidics are highly integrated on a tiny chip for novel functionalities.

B. Microfluidic flow cytometer, μFACS

There are many compelling reasons to create a compact, low-cost, chip-based flow cytometer, especially one with cell sorting capabilities (i.e., FACS systems). Currently, both cytometers and FACS systems are located in centralized facilities and shared by many users due to their high cost, large size, and significant cost for maintenance. Such centralized facilities impose limits on the accessibility of these powerful tools. In addition, traditional benchtop sorters are often droplet-based and thus exposed to air, increasing the possibility of generating biohazardous aerosols. Moreover, typical cytometers require relatively large volumes of sample and reagents for analysis, further increasing the total cost per run and creating difficulties in realizing certain applications. Each of these concerns limits the full utilization of the benchtop flow cytometer (FACS) system in various biomedical and clinical applications, in spite of its powerful capability to rapidly and quantitatively analyze biological samples.

Lab-on-a-chip microfluidic flow cytometers hold promise to overcome each of the above-mentioned difficulties. Their small size and potentially low cost promote portability and affordability by individual laboratories and point-of-care clinics. This is important for obtaining fast, accurate results. Numerous studies indicate that blood transportation time and handling can significantly affect test results;[14,15] thus, on-the-spot test can help produce more consistent and reliable results. Readily transportable devices can be deployed for testing in remote and resource poor locations, such as battlefields or underserved rural areas where medical testing is not widely available. Microfluidic flow cytometers can operate with small sample (and thus reagent) volumes, lowering the cost of assays and experiments. A mass-producible device would be more widely accessible to both research laboratories and clinics, yielding faster assay turnaround and enabling real-time studies. An integrated optical system would have fewer problems than current systems based on bulk optics. In fact, a highly integrated chip-based approach would turn much of the time consuming and expensive work of troubleshooting into simple chip replacement; and the probability of hardware failure will be reduced with the optical components integrated together onto a single chip. This should significantly reduce or eliminate the need for costly service contracts and dedicated maintenance personnel. Most importantly, however, an optofluidic flow cytometer offers the potential for innovative architectures and increased functionality that is simply impossible for conventional benchtop systems. The high level integration, along with parallel processing techniques, can be exploited for higher throughput screening, even with lower flow speeds. A closed sorting system reduces potential biohazard risks. Combined with the ability to integrate functionalities such as fluid pumping, sample preparation, cell culture, and reagent metering and mixing, the development possibilities for true lab-on-a-chip or micrototal analysis systems (μTAS) are endless. These are just a few of the reasons that, over the past decade, researchers have strived to miniaturize the flow cytometer onto a compact and portable chip. While the most advanced microfluidic flow cytometers may not be ready to replace traditional benchtop cytometers in the clinic just yet, the necessary technologies to realize this goal are growing fast, bridging and in some regards even over-reaching the gap between the commercial benchtop systems and the rapidly developing microfluidic platforms.

There are three core components of benchtop flow cytometers that need to be miniaturized while maintaining performance: (1) the fluidic system for introduction and placement of biological samples, (2) the optical system for illumination of samples and collection of emitted light (both scattered and fluorescent), and (3) the sorting system for deflection of samples of interest, which requires both real-time control and a rapid-response actuation system. The key challenge to developing high-performance miniaturized flow cytometers is to figure out how to reduce the volume and cost of these three systems while maintaining adequate performance (e.g., detection sensitivity and sorting throughput). In this article, we look at the major progress toward miniaturizing and integrating these three aforementioned systems. Along the way, we also introduce some recent developments in microfluidic flow focusing, on-chip light detection, and high throughput sorting capabilities from our own laboratory.

II. REVIEW ON RECENT ADVANCEMENT ON MICROFLUIDICS

In flow cytometry, consistent positioning of samples by flow focusing (e.g., sample confinement) is required to enhance cell sorting purity and to reduce variations in detected signal intensities. Samples are required to travel at a uniform speed to reduce significant variations in signal intensity resulting from illumination nonuniformity. Consistent placement also minimizes the possibility of coincidence events and false-sort incidents. Researchers have made great efforts in developing effective and elegant focusing methods.

Reynolds number (Re) is frequently involved to characterize different flow types,

$$\mathrm{Re} = \frac{\rho \mathrm{VL}}{\mu},$$

where μ is the fluid dynamic viscosity, V is the average velocity of the fluid, ρ is the fluid density, and L is the characteristic length of a rectangular channel or the diameter of a circular channel.[16] At the microchannel scale, Re is much smaller than 2000, thus flow is generally smooth and predictable, i.e., laminar flow. This dimensionless number also indicates the relative importance of viscous forces compared to inertial forces. When Re is extremely low (i.e., $\mathrm{Re} \sim 0$), the Stokes flow approximation is made, deeming inertial forces to be negligible. Microfluidic systems in this realm offer the benefit of highly predictable behavior that does not depend on sample size desirable qualities for a microfluidic sample positioning system. Numerous structures[17–25] have been designed for hydrodynamic flow focusing under this approximation and will be discussed in Sec. II A. More recent studies have made great progress in understanding the regime where Re is finite (i.e., at higher flow rates or smaller channel dimensions), a regime requiring inertial effects to be taken into account. This understanding of the resulting effects of secondary turbulent flow and inertial migration have led to the development of novel methods of generating three-dimensional particle focusing in microfluidic channels, which are reviewed in Sec. II B.

A. Hydrodynamic focusing

When fluid flows in a pipe, surface friction will cause the fluid flow located closest to the walls to travel much slower than the fluid flowing through the center. The flow velocity profile thus follows a parabolic distribution, meaning that particle velocity depends on relative position. For microfluidic flow cytometers, then, if the sample flow is not confined to the center of the channel, the fast-moving particles in the center of the flow can “catch up” to slower particles near the wall. For detection, the result is variation in illumination dwell time (or collection integration time), resulting in measured intensity variations between otherwise identical samples. For sorting, the result is a reduction in sort purity or “false-sorting.” Focusing samples to the center of the channel addresses both of these issues.

Hydrodynamic focusing is the most widely used flow confinement technique. For microfluidic devices, this confinement is typically two-dimensional, while three-dimensional flow focusing is exploited in benchtop flow cytometers. By adjusting the relative pressure between the sample flow line and the two flanking sheath flow lines, the sample flow can be confined into a narrow stream, as demonstrated in Fig. 2.[16] Using this approach, Knight *et al.*[20] demonstrated that an approximately 50 nm sample flow stream can be achieved in a 10 μm flow channel. Alternatively, hydrodynamic flow focusing can be achieved by applying negative pressure at the outlet and creating the flow rate differences via channel geometry (i.e., inducing a relative difference in flow resistance).[22] This allows fluid focusing using a single pumping source. In a related approach, air can be used as the sheath fluid to confine the sample flow while reducing the volume of the clean water needed.[18] Two-dimensional flow focusing constrains the sample flow in the lateral direction; however, the fluid velocity still exhibits a parabolic velocity profile in the vertical direction.

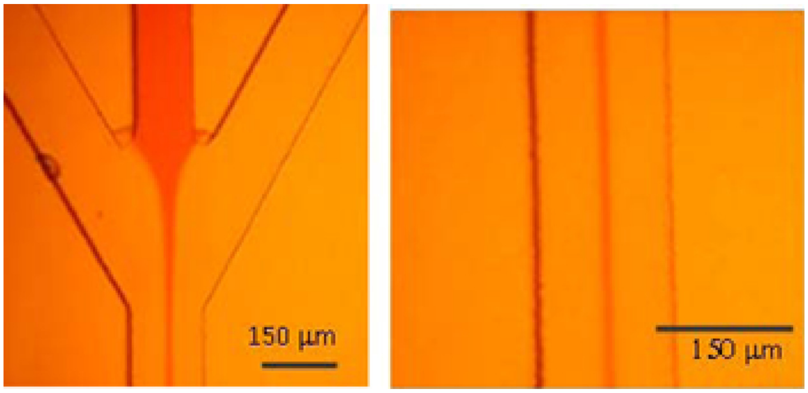

FIG. 2. Sample flow from the center inlet is focused by sheath flow to 20 μm width. The flow rate ratio of sample flow to sheath flow is 1:10. (Ref. 9).

Particles flowing near the top or the bottom surface of the microfluidic channel will travel slower than the particles moving in the center, resulting in the same problems mentioned above. That is, two-dimensional flow focusing will reduce, but not solve, the confinement problem.

In order to achieve three-dimensional flow focusing, Goranovic *et al.* designed a "chimney" structure to achieve a coaxial sample sheathing by injecting a sample flow into the sheath flow in a perpendicular direction.[19,24] Groisman and other groups fabricated multilayered, three-dimensional microfluidic devices to achieve confinement in the vertical direction.[17,21,23,25] However, these techniques have not been widely adopted in practice due to increased complication in fabrication process or the need to increase overall fluid flow rates (and thus overall particle velocity).

To exploit the effects of vortices generated by volume changes, microchannels can be fabricated with contraction and expansion regions. Howell *et al.* made chevron-shaped grooves [Fig. 3(a)] in the top and the bottom of the channel to "wrap" the sheath flow around the sample flow. They developed a microfluidic flow cytometer in which the sample fluid was thus confined to a small volume ($20\times34\times30\ \mu\mathrm{m}^3$) to reduce variations in detection signal intensities.[26] Similarly, Lee *et al.*[27] used a contraction-expansion array microchannel [Fig. 3(b)] to achieve three-dimensional flow focusing in a single-layer device. By modulating the flow rate and the number of contraction regions, they could control the focused position of the sample stream.

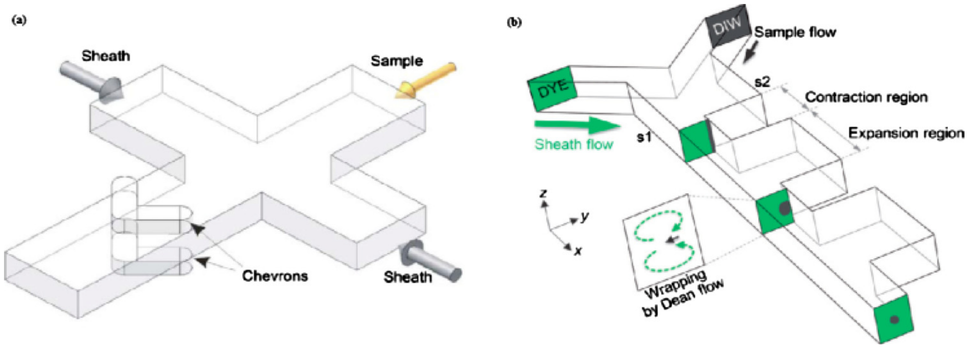

FIG. 3. The schematic design of (a) a chevron-patterned device (Ref. 26) and (b) the contraction-expansion array (Ref. 27) for three-dimensional flow focusing.

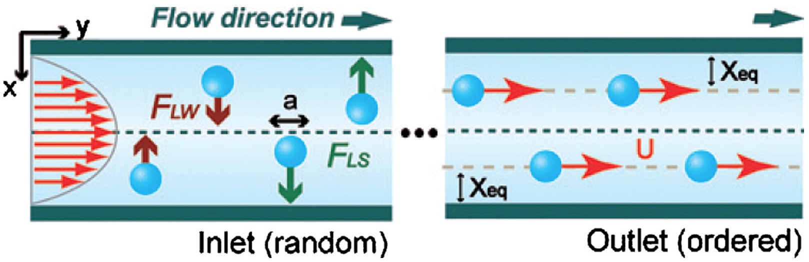

FIG. 4. Particles experience two lateral forces, wall effect lift (F_{LW}) and shear gradient lift force (F_{LS}), resulting in migration to the lateral equilibrium positions (X_{eq} away from the top and bottom surfaces) inside the microfluidic channel (Ref. 29).

B. Inertial effect (nonzero Re)

When Re is small but finite (e.g., $\sim 10^{-1}-10^{2}$), inertial forces can no longer be neglected. Researchers have utilized the inertial effects in both straight and curved channels to perform three-dimensional particle focusing, cell sorting, fluid mixing, and other functionalities. An excellent review paper on the recent advancements in inertial microfluidics by Di Carlo[28] is highly recommended for the readers who are not familiar with the inertial effect in microfluidics channel. In the case of a simple straight channel, a rigid particle flowing through a microfluidic channel will experience two counterdirectional lift forces, one due to a "wall effect" and the other the result of the shear gradient due to the parabolic flow profile (i.e., Poiseuille flow).[29] The result of the balance of these forces is the existence of specific equilibrium positions, generally away from the center of the channel, that the samples will migrate toward as they flow through the channel (as shown in Fig. 4). The equilibrium position of particles depends on the geometry of the channel and the size of the sample in flow, among other parameters. Using these effects, Park[30] designed a multiorifice microchannel to focus particles to either the center or the side of a channel, depending on the particle Reynolds number.

One benefit of exploiting inertial effects is the possibility of massively parallel sample focusing without added hardware (i.e., multiple pumps). Hur *et al.*[29] introduced a sheathless and label-free parallel flow cytometer to increase the throughput for analyzing rare samples in dilute solutions. They constructed a single inlet, which is split into 256 channels, so that the injected cells are positioned and spatially ordered by inertial effects, as shown in Fig. 4 below.[31] Their device allows easier operation, accurate detection, and differentiation of cells at higher sample concentrations than traditional flow cytometers will allow, while operating at a throughput of around 1×10^{6} cells/s (over ten channels).[32]

Most recently, Oakey *et al.*[33] fabricated a staged device including both curved and straight channels to confine particles into a single streamline without sheath flow (Fig. 5). They further demonstrated that a flow cytometer equipped with this staged structure exhibits performance competitive with that of a commercial cytometer with standard hydrodynamic focusing. The device is easy to fabricate and eliminates the need for sheath fluid and additional syringe pumps, significantly reducing the size of the external fluidic control system. Their device can operate at higher flow rates, which is ideal for high throughput flow cytometry analysis; moreover, the inertial focusing with the staged structure enables for the high resolution comparable to a commercial flow cytometer. Their work suggests a significant role for inertial focusing in the development of inexpensive lab-on-a-chip flow cytometers, particularly in applications requiring the analysis of high sample concentrations and high purity sorting of pure subpopulations.

III. MINIATURIZATION OF OPTICAL DETECTION SYSTEM

As stated previously, the optical system of the flow cytometer must perform two functions: illumination and collection. For illumination, we require a small spot size ($\sim$20–60 μm wide),

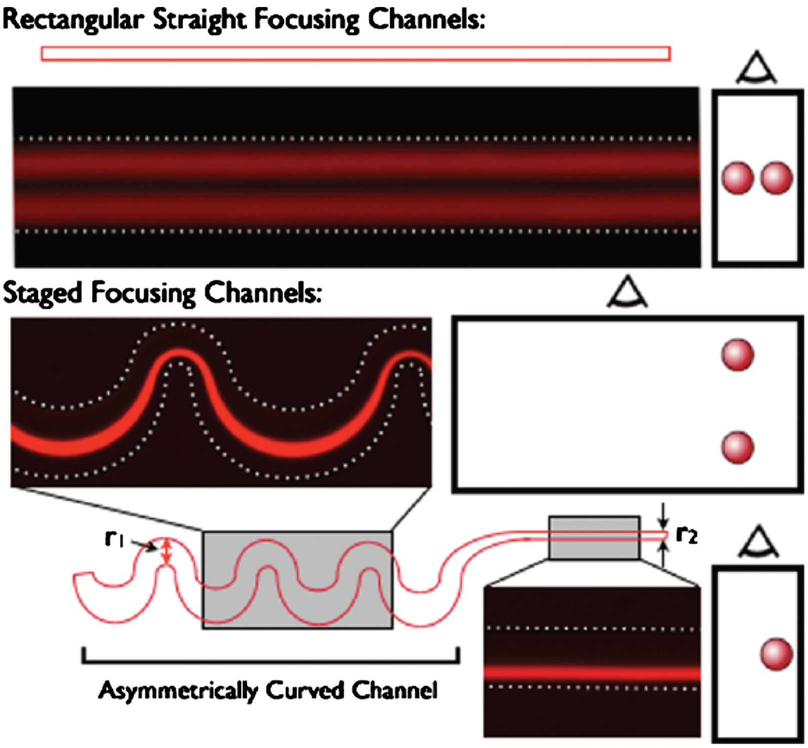
Rectangular Straight Focusing Channels:
Staged Focusing Channels:
r1
r2
Asymmetrically Curved Channel

FIG. 5. Schematic of the inertial focusing process in an asymmetrically curved channel followed by a straight channel. The combination of the curved and the straight channels in series biases the particles in the fluid to one half of the channel. As a result, the particles are focused to a single vertical streamline within the straight channel (Ref. 33).

spatial uniformity, and collimation or near-collimation. These requirements increase throughput, reduce variation, allow angular light scatter measurements, and reduce "noise" from stray light. For light collection, *localized* light collection is important; the system must collect light from the location of the interrogated sample (hence, the attention to flow focusing) and reject light from other locations (i.e., sidewall reflections, scatter from passing debris in the sheath fluid, etc.). Such localization of collection is imperative for adequate signal-to-noise ratios in the collection system. This is especially true in light scatter measurements, as wavelength filters cannot be employed to reduce stray light. Indeed, most flow cytometers are set up such that angular light scatter intensity levels are more than sufficient for detection of even subwavelength particles; detection is often limited not by signal intensity, but rather by background collection.[34]

In microfluidic chips with integrated optical systems, waveguides and/or optical fibers are often employed to route or guide light on the chip based on total internal reflection (TIR). Off-the-shelf fiber optics are readily integrated into microfabricated devices.[35–39] Frequently this is accomplished by the use of a fiber sleeve,[35,37–43] which guides fiber insertion to correctly position the fiber (see Fig. 6). The sleeve guarantees coarse fiber alignment; however, there is likely to be some rotational and translational variation from device to device. Other approaches include aligning the fiber and then using some sort of fixative (polymer, epoxy, etc.) to stabilize the fiber.[36] Fiber optics are often used to easily interface with a prototype device (or with the device's waveguides), with the idea that in the future dedicated hardware (a chip reader) would be used to interface seamlessly with the commercialized version of the proposed device, in lieu of fiber optics.

A more permanent solution can be found in integrated waveguides (Fig. 6). These can be created in a number of ways, such as by using photoresist[44,45] or another high refractive index material to define waveguide cores that are then cladded by surrounding air pockets. As microfluidic chips are often created as mold-replicated devices, another common means of creating

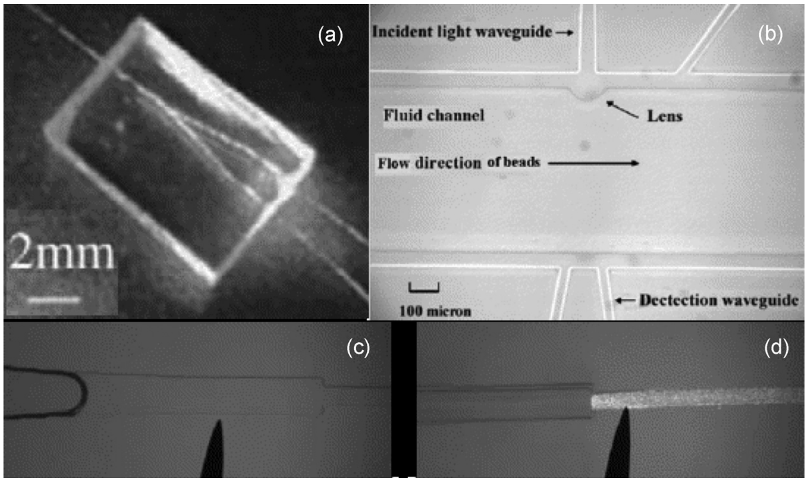

FIG. 6. A variety of methods to incorporate optical elements: (a) integrated waveguides forming a y-splitter in PDMS (Ref. 48), (b) a lensed waveguide facet for altering beam divergence (Ref. 45), (c) a fiber sleeve filled with PDMS prepolymer for waveguiding, and (d) the same sleeve with an optical fiber inserted (Ref. 39).

integrated waveguides is to fill a "channel" in the device with a higher index material, such as polydimethylsiloxane (PDMS)[35,46,47] or any of various high-index liquids,[48] creating a light-guiding core relative to the lower-index device body material. In each case, the waveguide structure is generally created monolithically alongside the microfluidic flow channel, requiring few additional steps (generally just a filling step) and no alignment. Thus, waveguide integration adds great functionality to the device at little to no added cost. Often, for prototyping, some of the above-mentioned fiber integration methods will be used to interface the waveguides to the outside world.

While fibers and lenses offer a good start to optical system integration, they are not a complete solution, as TIR-based light-guiding optics (i.e., both fibers and waveguides) emit a diverging cone of light. For interrogation optics, this means an uncollimated (less directional and nonuniform) illumination beam. For collection optics, this means that the collected light consists not only of the cone of light originating from the cell of interest, but also any other light incident on the waveguide that satisfies the TIR requirements. That is, by nature, waveguide- or fiber-only systems do not inherently collect light from a localized area (the cell of interest) in the way that a standard imaging system would. Any collected light originating from some location other than the cell of interest is noise, and without a method of restricting the collection of this light, the resultant noise can significantly degrade the performance of the optical system. Published sample coefficient of variation (CV) from microfluidic devices with fiber- or waveguide-based optical systems appear to reflect this issue (the effects of which are often worsened by single-dimension flow focusing).[45,49,50] In such devices, polystyrene beads with expected CVs of under 10% (generally ~3%–5%) are typically measured to have scatter CVs of 25%–35%. While such devices demonstrate the utility and possibility of integrated optics, practically speaking, we must reduce the extrinsic variations resulting from excess background collection (as well as the issues arising from incomplete flow localization, as discussed previously).

Simple refraction (Snell's law) can be used to change the light path by "lensing" a fiber or waveguide facet (Fig. 6). The divergence of the illumination light could thus be reduced, moving toward a collimated or even focused output. Similarly, a lensed collection fiber (or waveguide) could be made to collect light from a more localized position. Camou *et al.*[40] demonstrated lensed fiber sleeves to reduce beam divergence, increasing the intensity of the illumination beam. Similarly, a lensed waveguide facet has been demonstrated by Wang *et al.*[45] to change the diverging light beam into a converging light beam, reducing the length of the cell interrogation zone and increasing the illumination intensity. This single lensed surface approach then provides a means of

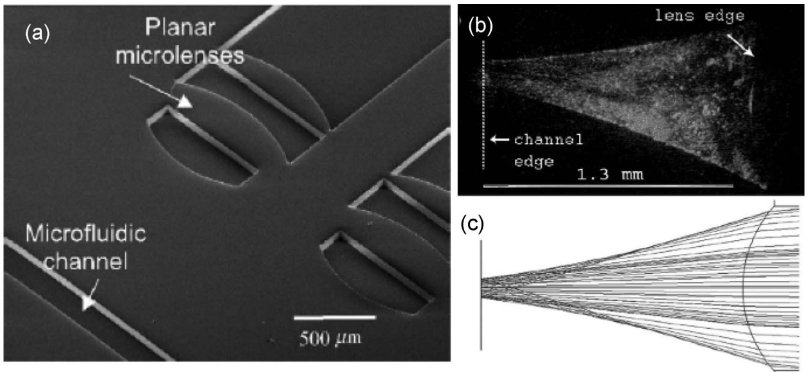

FIG. 7. Freestanding integrated lenses: (a) air-filled lenses created in PDMS (Ref. 51), (b) image of light tracing (via alumina scattering centers) from a fluid-filled lens in PDMS, and (c) the corresponding optical modeling for the lens based on shape and refractive index (Ref. 46).

reducing the width of the diverging illumination beam to more efficiently interrogate the sample. Because the fiber (or waveguide) is not a point source, however, the light path cannot be focused to a point and cannot be well-collimated. To create a more well-collimated or well-focused light path, the source needs to approximate a point source; i.e., a larger lensed surface needs to be positioned farther from the light source. To do this, we require "freestanding" lenses.

Freestanding two-dimensional lenses can be readily incorporated into many microfluidic chip (Fig. 7). As mentioned above, all of the features in mold-replicated devices are created monolithically and in fixed alignment by simply transferring the pattern from a mask into the mold material. The optical functionality of such molded features is determined by shape and refractive index. With regard to the shape, there is a great deal of design flexibility to work with. Two-dimensional lenses are readily formed by including a lens-shaped pattern on the mask, which translated to a lens-shaped cavity in the device. Much like the waveguide cavity was filled with a high refractive index material to allow it to guide light, the lens-shaped chambers will be filled with a high refractive index material so that, relative to the lower-index device body, they act similarly to a traditional glass-in-air lens. Beam diverging lenses can also be created and filled with a low index material (e.g., air) to create the same effect with the opposite refractive index contrast. Note that lenses created in this manner can have any spheric, aspheric, or parabolic curvature desired. This is a stark contrast to bulk lenses, where such customized shapes can require individual diamond-turning, making them very costly. Figure 7 shows two-dimensional lenses, both air-filled[51] and liquid-filled,[46] integrated into microfluidic chips by simple molding process. Seo and Lee[51] demonstrated a significant increase in excitation efficiency by using integrated air-filled lenses to confine and collimate the illumination beam. Godin and Lo[52] demonstrated the use of integrated lenses for efficient collection of scattered light in a specific range of angles.

The methods of integrating lenses described above thus allow highly customized optical system design while producing fixed-alignment optical systems in an inexpensive fashion. However, the approach also faces some significant challenges limiting the device performance. First, the lenses are generally two-dimensional (although some attempts at developing three-dimensional lenses have been demonstrated[53]), thus the light path is unaffected in the vertical (out-of-plane) direction. In addition, lenses require optical-quality facets (rms roughness of ~1/10 of the wavelength) and near 90° sidewall angles. This requires well-controlled photoresist processes, specialized silicon etch processes,[54] the development of a postetch sidewall-smoothing process,[55] or similarly meticulous processing. Lastly, lenses created in this manner cannot be antireflection coated, meaning that even with a perfectly smooth surface, a per-surface Fresnel reflection loss still exists. This can be mitigated by reducing the refractive index contrast, but at the expense of lens power. The result is a limit on the number of lenses that can feasibly be included in an integrated optical system.

An alternative (or supplemental) approach to a lens-based optical system may include an exclusion-based approach to light collection, that is, finding some means of further shaping the divergent light path from a waveguide, or further restricting the light that a waveguide collects, to provide more localized illumination and collection without necessarily requiring lenses. As a supplement to more typical optical systems, this approach can involve ideas such as spatial filtering[34,56] or other means of stray light-blocking to enforce more highly localized light collection. Several authors have demonstrated integrated light-blocking elements. Once again, the feature is included on the photomask and transferred into the mold, creating a "chamber" in the device. By filling this chamber with ink, both Tang *et al.* and Ro *et al.* demonstrated spatial restriction of the illumination beam.[39,57] Solid-filled apertures have also been demonstrated using an off-the-shelf opaque PDMS polymer (similar to creating polymer-filled waveguides, but with a gray-black polymer).[58] In addition to light-blocking elements, light excluding elements can also be created by exploiting TIR optics and the unique geometries afforded by microfabrication. One such device is discussed in Sec. III A.

While the above discussion is primarily concerned on devices where the illumination path crosses the fluidic path, there are other cases where we want both the light and the fluid to share the same path in order to maximize their interaction. Several optofluidic waveguide structures coconfining photons and fluids in microchannels have been reported. The Whitesides group[59] demonstrated liquid-core and liquid-cladded waveguide structures, and Yang group demonstrated liquid-core and air-cladded optofluidic waveguides.[43] Without three-dimensional focusing, however, light will be lost along z-direction in both methods. Cho *et al.*[60] reported liquid-core and solid-cladded optofluidic waveguide structures by coating Teflon AF onto the microfluidic channel wall. Since Teflon AF has lower refractive index ($n=1.29-1.31$) than that of PDMS (≥ 1.41), the introduced light can be confined and guided by total internal reflection three-dimensionally (even if the fluid is only confined two-dimensionally), thus minimizing propagation loss. In this way, fluorescently labeled samples can be excited throughout the channel length with a single laser. Fluorescent emission can be detected at multiple spots, and as the fluid path is split, so is the light path, creating a fluidically controlled optical circuit. This technology offers design flexibility and efficient interactions between light and biological samples for laboratory-on-a-chip devices, thus enhancing detection sensitivity. Illumination along the length of the channel can now be applied to a highly integrated microfluidic flow cytometer, enabling space-time coding technologies,[56,61] as will be discussed in Sec. IV B. Such optofluidic waveguides further enable color-space-time (COST) coding (see Sec. III B), a novel way to detect multiple fluorescent wavelengths using a single photodetector.[62] Here, the focus is on minimizing the size and cost of not just the chip, but also the surrounding optical detection system as well. This method of discriminating multiple fluorescent colors with a single PMT, pioneered in our laboratory, holds great promise to significantly reduce the cost and size of the total system.

A. Exclusion-based optical systems

In our laboratory, recent advances in integrated light scatter collection techniques have achieved forward scatter CVs as low as 8% (even with only two-dimensional flow focusing), and have made possible the inclusion of both forward scatter (FSC, here approximately 3°–12°) and side (orthogonal, here approximately 92°–98°) scatter (SSC) optics in the plane of the device. Typically fluid flow, illumination/FSC lines, and SSC lines are mutually perpendicular, but in the chip-based architecture there are only two dimensions in which to integrate features. In our device, the flow channel passes by the illumination waveguide at an angle a bit beyond perpendicular. This relatively small tilt (~16°) keeps the resulting reflection losses low while creating sufficient space for a scatter collection line orthogonal to the direction of illumination. By slightly separating the interrogation locations for the FSC and SSC collection lines, incorporating the SSC line becomes even easier, as the effective illumination directions at the two collection locations are slightly different.

As mentioned above, this recent work also relies heavily on an exclusion-based approach to light collection. In these devices, shown in Fig. 8, formerly flat-faceted waveguides are redesigned

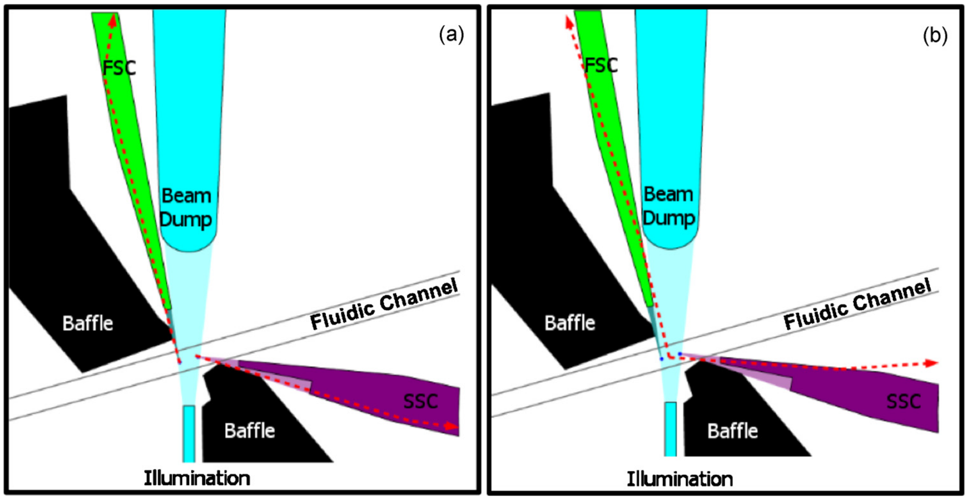

FIG. 8. Schematic of a microfluidic cytometer design based on exclusion optics. Light originating from either of the two interrogation points (circles in fluidic channel) couples through a flat facet into the collection waveguides. Light originating between these points (or outside of them) is incident on an angled facet, experiencing significant reflection losses as well as a path change that will drastically reduce waveguide coupling (Ref. 63).

and reshaped to have a conical taper that ends in a rather small flat entrance facet close to the fluidic channel. The result is that light scattered from the cell is collected through the flat facet and is generally unaffected by this waveguide change [Fig. 8(a)], whereas light originating from other locations will generally pass through the angled sidewall of the newly extended waveguide. The angled facets utilize a combination of high reflectance (due to low-angle incidence) and change of transmission angle (due to refraction) to alter the light path of this noise, preventing coupling into the collection waveguide [Fig. 8(b)]. The results are reduced cross-talk between cells close to one another and reduced background light collection. This approach is specifically enabled by the use of a microfabrication platform, which allows small, high precision geometries located in close proximity to the sample. Such designs have potential to significantly reduce reflective losses, as (a) fewer (lens) surfaces are required, (b) the "optics" operate at a lower-index contrast (as lens power is not necessarily important for this type of optic), and (c) light from the cell is generally incident normal to the surface of the optic, further reducing reflective and scattering losses. The result is a drastically simplified optical system that retains spatial discrimination capabilities.

This device was benchmarked using 5, 10, and 15 μm polystyrene beads. Clear separation of the three bead populations was observed. The FSC CVs are 8%, 10%, and 29% for the 15, 10, and 5 μm beads, respectively. The increase in CV with decreasing diameter is likely due in part to the flow focusing (apparently to a width of >5 μm) and in part to the signal intensity approaching the noise limit for this device and detection setup. The SSC CVs from this device are 25%–38%. While these CVs seem relatively large, the SSC CVs from the commercial device are actually quite large as well, 18%–22%. Work is underway to further reduce the scatter CVs through better flow focusing, lower-noise detectors, and further reductions in stray light. In the current state, however, the scatter CVs are among the best demonstrated by integrated optical systems, and are sufficient to allow discrimination of the three bead populations. Furthermore, compared to an effectively identical system created without the tapered features to the waveguides (i.e., flat facet only), the FSC signal-to-noise ratio was improved by a factor of 10, clearly demonstrating the improvement in collection localization afforded by this system. The approach employs far fewer surfaces than lens-based designs, and offers far better localization of light collection than other lensless designs (such as standard flat-faceted waveguide approaches).

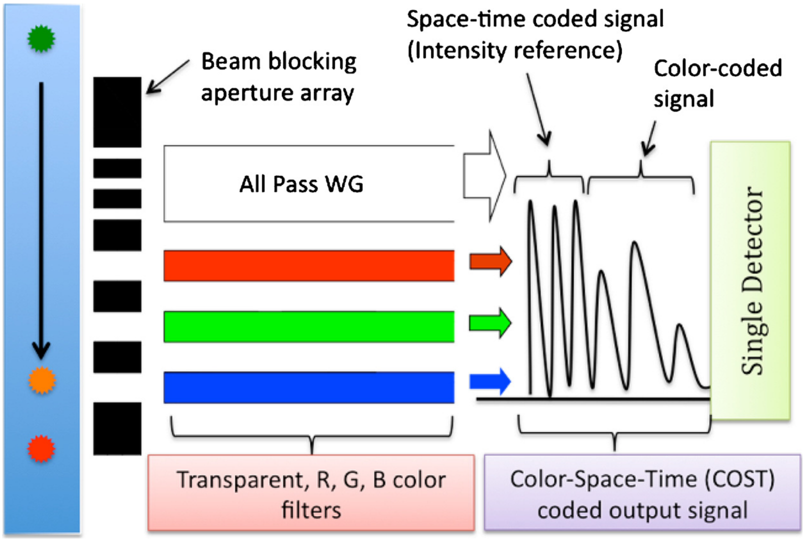
Beam blocking aperture array
Space-time coded signal (Intensity reference)
Color-coded signal
All Pass WG
Single Detector
Transparent, R, G, B color filters
Color-Space-Time (COST) coded output signal

FIG. 9. Schematic illustration of COST coding technology device structure. Each fluorescence color is first temporally coded by the spatial pattern of the first three beam blocking apertures. Next, the color is encoded by the red, green, and blue color filters and the associated spatial filter (apertures). The COST-coded color fingerprint is unique to each color, enabling multicolor registration by a single PMT (Ref. 62).

B. Multicolor detection employing COST coding technology

In the field of flow cytometry, there is a constant drive to increase the number of distinct measurements for each cell. As each fluorescence band corresponds to a distinct fluorescence-based measurement of an individual cellular protein or function, the quality and quantity of flow cytometry measurements can be significantly enhanced by the availability of additional fluorescent labels. Thanks to the coordinated successes in developing new hardware, fluorochromes, and software tools, the most advanced systems can measure as many as 17 fluorescent colors, finding applications in immunophenotyping or stem cell research.[10,11,64] Unfortunately, the detection of so many fluorescence colors requires essentially an equal number of dichroic mirrors, optical filters, and PMTs, all adding to the size, weight, and cost of the system. This is the key reason that today's benchtop flow cytometers are still bulky and costly, thus having only limited use for point-of-care applications. For flow cytometers, a significant part of the attraction of the lab-on-a-chip approach is the reduction in cost and size of the system, which ultimately means dramatically reducing the bulk optics, and most important, the number of PMTs the system requires.

To overcome the one-PMT-per-fluorescence-color limitation, our group has developed a novel fluorescence color detection technology, dubbed COST coding, for lab-on-a-chip flow cytometry applications.[62] The technology mimics the working principles of human eyes, which can distinguish more than 1000 colors using only three types of photoreceptor cells.[65] In the somewhat analogous COST coding method, a fluorescence emission signal is encoded into a time-dependent signal as each fluorescently tagged cell passes by an on-chip spatial and color filter waveguide array. The scheme effectively uses the temporal coding created by the spatial filter, combined with integrated broadband color filters, to encode for a spectral signal in the time domain, as illustrated in Fig. 9.

The first three identical peaks are "space-time" coded signals and set the reference intensity of each detected fluorescence signal for accurate signal comparisons. The following three peaks, each with different intensities, are "COST" coded signals, which create the unique color fingerprint of each fluorescent color.

The on-chip spatial filter (i.e., the beam blocking aperture array in Fig. 9) is fabricated by filling the aperture cavity with blackened PDMS (Sylgard 170, Dow Corning). The three color filters (red-green-blue) are fabricated by filling the channels with material mixed with specific

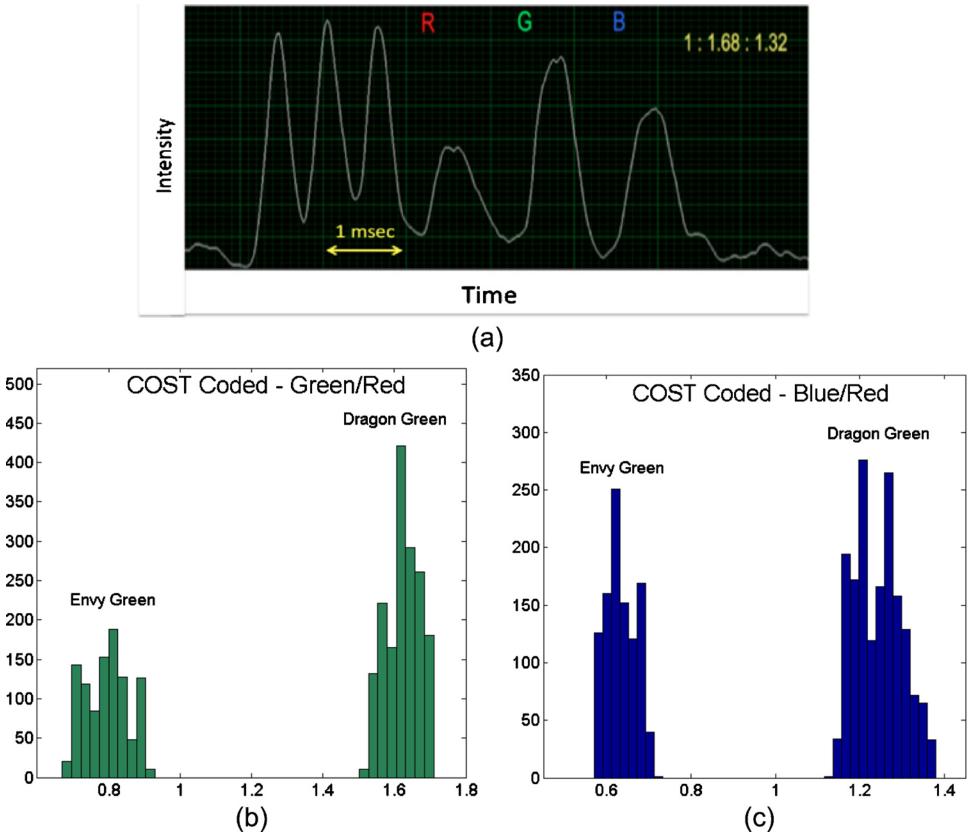

FIG. 10. (a) COST-coded output waveform of dragon green fluorescence. The first three space-time coded signals are followed by three color-coded peaks of different intensities. (b) Histogram of the green filtered COST-coded signal normalized to the red filtered signal of dragon green and envy green fluorophores. (c) Histogram of the blue filtered COST-coded signal normalized to the red filtered signal of dragon green and envy green fluorophores (Ref. 62).

dyes. Glycerol is used as the base material for the core of color filter waveguides, as it is optically transparent and exhibits a higher refractive index ($n=1.47$) than the cladding PDMS ($n=1.41$). Appropriate dyes are mixed with the glycerol to form the red, green, and blue broadband color filter waveguides.

To distinguish as many fluorescent colors as possible, each color waveguide is designed to possess a gradual slope in its transmission spectrum, similar to the transmission spectra of photoreceptors found in the combs of human retina.[65] In contrast with conventional bandpass filters with sharp, narrow transmission windows, these more gradual wideband color filters reduce the required number of filters to differentiate multiple colors. The fluorescence color information is encoded in the relative signal intensity registered by each color filter waveguide, the same principle that has been manifested in the human eye.

Applying the COST technique, we have demonstrated that two widely used fluorescent species—dragon green (emission peak at 520 nm) and envy green (emission peak at 565 nm)—can be distinguished using a single PMT. Figure 10(a) shows the waveform of a COST-coded signal from the dragon green dye (equivalent to fluorescein isothiocyanate (FITC), a fluorochrome commonly used in flow cytometry). The first three peaks establish the reference for the fluorescence intensity, followed by the three color-coded peaks of different intensities. Figure 10(b) shows the histogram of the green/red ratio from beads labeled with either the dragon green or the envy green fluorophores. Similarly, Fig. 10(c) shows the histogram of the blue/red ratio of these two groups of fluorescently labeled beads. It is clearly shown that these two fluorophores can be differentiated with a single PMT by using the COST coding employed in this device. In fact, our analysis shows

TABLE I. Sorting performance of most common μFACS.

Reference	Sorting principle	Analyte used	Sort rate[a] (cells/s)	Detection throughput (cells/s)	Enrichment factor (fold)
Reference 71	Electro-osmosis	*E. coli*	⋯	20	30
Reference 70	Electro-osmosis	Beads	10	<1	70
Reference 72	Dielectrophoresis	Beads	Up to 300	10	⋯
Reference 73	Optical	HeLa cells	250–500	⋯	63–71
Reference 75	Hydrodynamic	⋯	5	⋯	⋯
Reference 24	Hydrodynamic		400	12 000	100
Reference 74	Hydrodynamic	*E. coli*	200	⋯	90
Reference 61	Piezoelectric-actuated	Beads and K562 cells	1000–10 000	>1000	200 (beads), 230 (K562 cells)
Reference 76	Piezoelectric-actuated	*E. coli*	1000–10 000	>1000	223

[a] Theoretical maximum sort rate.

that by using the COST technology, we can differentiate 11 commonly used fluorophores in flow cytometry by using a single PMT,[62] a major step toward the realization of compact, cost effective, and multicolor flow cytometers for point-of-care applications.

IV. MICROFLUIDIC FLUORESCENCE-ACTIVATED CELL SORTER (μFACS)

Traditionally, researchers study cellular activities from a cell colony containing a relatively large number of cells (i.e., 10^3-10^6 cells), yielding data that represent the general (bulk) behaviors of cell populations. Even though cells may appear to be similar morphologically, cellular heterogeneity (e.g., differences in gene expressions, cell proliferation, and responses to external stimuli) exists both in bacteria and eukaryotic cells.[66–69] In order to recover the rich information (e.g., stochastic behavior of individual cells) from cell-based assays, it is essential to extract single cells from a population/subpopulation of cells. As a result of significant advances in microfabrication technologies, numerous microfluidic cell sorters exploiting various sorting actuation mechanisms (e.g., electro-osmotic,[70–72] optophoretic,[73] hydrodynamic,[24,74,75] piezoelectric,[56,61,76] etc.) have emerged (see Table I). Table II lists some of the benefits and detractions of these various sorting mechanisms that have been explored for use in μFACS systems. Since fluorescence-based assays have been one of the most commonly used bioanalytical tools for researchers, this paper will focus on mechanisms that are compatible with fluorescence-activated-cell sorting (FACS). For other nonfluorescence-activated cell sorting mechanisms, such as magnetophoresis[77] and acoustophoresis,[78] readers can refer to a number of recently published articles.[12,79–81]

A. Survey of μFACS

Electro-osmotically driven μFACS has been developed and implemented by a number of research groups due to its relatively easy fabrication process (insertion of platinum/gold microelectrodes) and straightforward fluid manipulation (application of dc voltage across inlets and outlets). The first generation of μFACS was developed by Fu *et al.*,[71] who fabricated a three-channel "T" design in PDMS to achieve sorting based on electrokinetic switching. As fluorescence from *E. coli* (made to express fluorescent proteins) is detected upstream, the triggering of dc voltage across an inlet and two outlets causes fluid switching, permitting targeted cells to reach the desired collection outlet. In this study, a sorting throughput of ~20 cells/s and a 30-fold enrichment factor were achieved. In a similar approach, another group demonstrated manual sorting of red blood cells by switching the applied voltage potentials (300–500 V) across the inlet and outlets.[82] Dittrich and Schwille described another electro-osmosis-induced sorting method by

TABLE II. Comparison between common sorting mechanisms.

Sorting mechanism	Pros	Cons
Electro-osmosis	Easy fabrication, simple control, uniform flow pattern	High input voltage (>100 V), ion depletion, low-cell viability, low throughput
Dielectrophoresis	Able to trap cells, low-cell damage, fluid flow-independent particle movement	Cell property-dependent, low throughput, requires use of buffer of different ionic strength, complex fabrication
Optical forces	Contactless manipulation, low-cell damage, fluid flow-independent particle movement, high purity	Limited throughput, extensive optical setup (including use of a bulky high-powered laser)
Hydrodynamic	High throughput ($>10\,000$ cells/s), low-cell damage, easy fabrication, high enriching capability	Slow response, requires bulky external actuators (e.g., external check valve, syringe pump, and pneumatic pump), low purity
Piezoelectric-actuated	High throughput ($>10\,000$ cells/s), fast response, low-cell damage, easy fabrication, high enriching capability	Medium purity[a]

[a] Purity can be significantly improved by adjusting the flow speed, cell concentration, and incorporation of 3D flow focusing.

implementing hydrodynamic fluid focusing before subjecting the sample fluid to a dc electric potential in a "Y" sorting junction (Fig. 11). By switching the polarity of the applied dc voltage at the sorting junction, the sample flow could be deflected either to the right or left channels.[70] The authors demonstrated a tenfold enrichment at a throughput of 1 cell/s. Electro-osmosis-based sorting generally suffers from ion depletion,[83] low throughput, high-power usage, and low-cell viability due to the use of high electric field.

Dielectrophoretic (DEP) μFACS employs a gentler electric field-based sorting mechanism by using ac voltage in the megahertz range. The direction of the DEP (i.e., positive or negative DEP) forces experienced by the analytes is determined by the relative polarizability between the surrounding fluid and the analytes (e.g., beads or cells). Unlike electro-osmosis, which achieves sorting by moving particles along with the fluid, DEP moves particles relative to the fluid motion. In the earlier work, DEP forces were used to trap cells of interest, such as in the eight-electrode quadrupole cage, to allow trapping of L929 cells.[83] Following this work, another research group designed and implemented arrayed quadrupole DEP traps to manually hold and isolate fluorescent cells against pressure-driven fluid flows.[84] While sorting throughput is low, the advantage of this approach is that biochemical assays can be readily performed on these trapped cells (as flow is

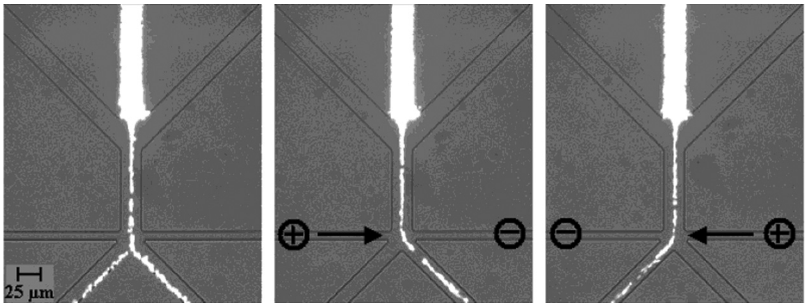

FIG. 11. Electro-osmosis-induced particle deflection. After hydrodynamic focusing, the highly concentrated fluorescent beads are deflected to the right or left collection channel, depending on the polarity of the applied voltage (Ref. 70).

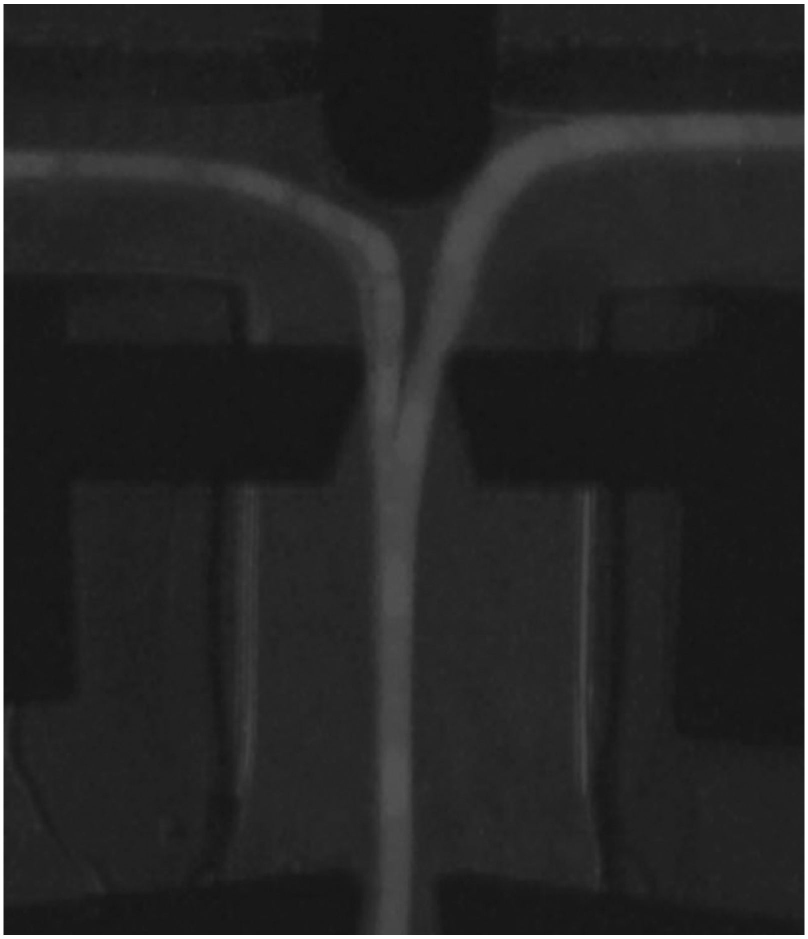

FIG. 12. Superimposed images of 200 particles passing through the sorting junction. After dielectrophoretic focusing, ~100 particles are deflected to each of the collection channels (Ref. 72).

permitted), allowing sorting and monitoring of cellular responses on a single chip. In addition to cell trapping, Holmes *et al.*[72] achieved particle deflection by embedding a two-electrode system oriented parallel to the flow, causing DEP forces perpendicular to the fluid flow (Fig. 12). The design enables deflection of individual beads at a rate of 300 beads/s under an applied voltage of 20 $V_{\text{p-p}}$ at 10 MHz. In an automated sorting system, the authors achieved an actual throughput of 10 particles/s. In fluorescence-activated DEP sorting, the throughput is limited because DEP forces are generally too small relative to the hydrodynamic drag force to rapidly deflect the cells from the flow stream. In addition, the fabrication process for a DEP cell sorter is fairly extensive, and most of the microfluidic DEP systems require buffer solutions of much lower conductivity than standard buffers. Finally, the DEP force has a third power dependence on the particle size. When the size of the particle is smaller than 1 μm, the DEP force is too small to be practical, thus DEP-based sorting cannot be applied to separate bacteria or viruses.

Optical forces have also been used for the trapping and sorting of living cells.[85,86] Wang *et al.*[73] demonstrated an optically controlled μFACS using an acousto-optic modulator controlled ytterbium laser (20 W) for cell manipulation (Fig. 13). Various mixtures containing green fluorescent protein (GFP)-expressing and non-GFP-expressing HeLa cells (ratios of 50:50, 10:90, and 1:100) were used to characterize the sorting performance. Sorting throughput of 20–100 cells/s and enrichment factors of 63–71-fold were obtained. Although the purity of the sorted samples was relatively high (most are >90%) compared to the results from other μFACS systems, the use of the bulky, expensive, high-power laser as well as the accompanying elaborate optical setup is

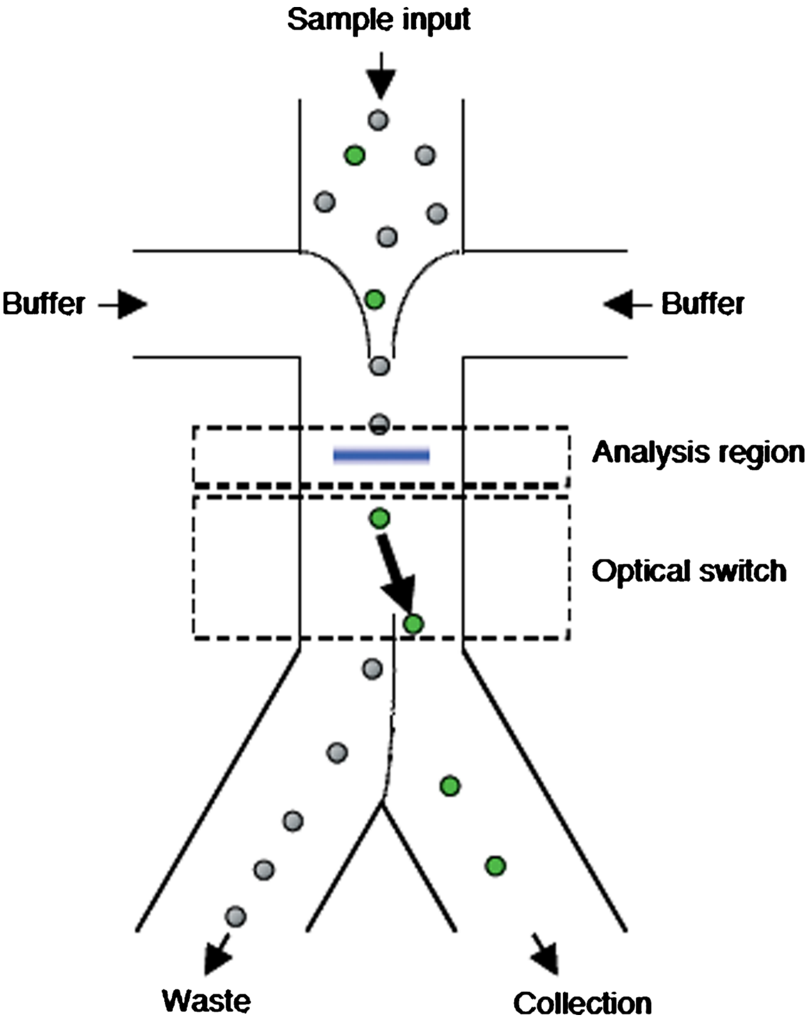

FIG. 13. Principle of an optical cell sorter. After sample focusing, cells are analyzed in the analysis region based on their fluorescence. The detected fluorescence triggers laser-directed cell manipulation, causing targeted cells to be sorted to the collection channel. All the nontargeted cells flow to the waste channel (Ref. 73).

unfavorable for miniaturization. Additionally, much like DEP sorters, the limitation on flow rates due to the relative weak optical forces seriously limits the detection throughput of optical μFACS systems.

Sorting based on hydrodynamic flow switching, on the other hand, is typically not limited by the flow (or particle) speed, and therefore the method generally produces a high detection throughput (>1000 cells/s). By manually controlling a syringe pump, Krüger *et al.*[75] redirected the flow from a waste channel to a collection channel. Due to the slow mechanical response of the syringe pump (~ 0.26 s), the maximum sort rate is only 4 particles/s.

Using a faster external check valve (response time of ~ 2.5 ms), Wolff *et al.*[24] demonstrated fluorescence-activated sorting by actuating the valve upon detection of targeted particles, as illustrated in Fig. 14. In this study, the authors sort 10 μm fluorescent beads from a mixture of beads and chicken red blood cells, achieving a detection throughput of 12 000 cells/s and an enrichment factor of 100-fold. Instead of employing external actuators for sorting, Fu *et al.*[74] integrated the PDMS membrane-based (~ 40 μm diameter) microvalves (~ 5 ms theoretical response time) on-chip to manipulate the fluid flow using multilayer soft lithography. The upper layer contains channels that are pressurized/vacuumed by an external pneumatic actuator, which in turn causes

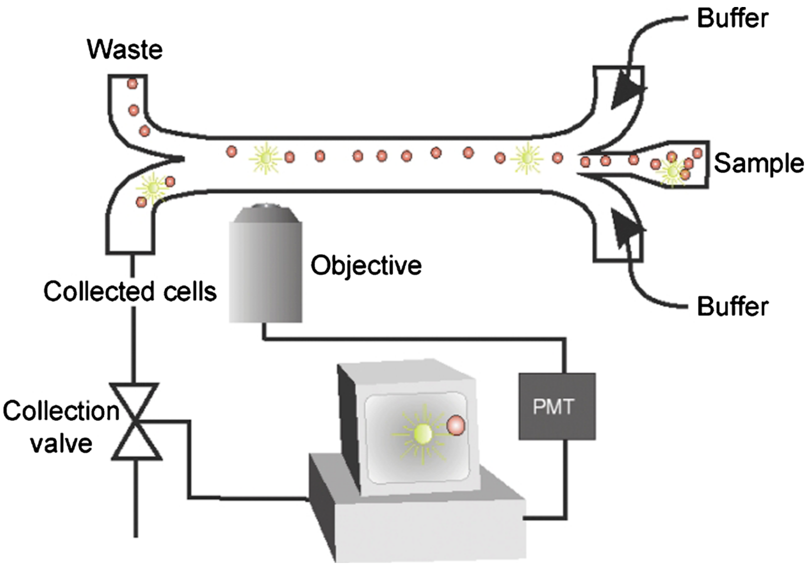

FIG. 14. Hydrodynamic flow switching using an external check valve. Upon detection of fluorescence from the sample, the electronic feedback system triggers the opening/closing of the check valve, causing sudden redirection of the fluid flow (Ref. 24).

the closing/opening of the microvalves. With the pneumatically actuated valves, a sorting throughput of 26–44 cells/s is achieved and the enrichment factor could be as high as 90-fold. Even though sorting based on hydrodynamic flow switching generally offers high throughput and enrichment capabilities, causes minimal cell damage, and is not subjected to buffer incompatibility issues, the mechanical actuators (e.g., external valves, syringe pumps, and pneumatic pumps) employed usually suffer from limited response times and are generally bulky, hindering progress toward miniaturization.

B. Integrated μFACS using an on-chip piezoelectric actuator

To circumvent the use of bulky actuators, Chen *et al.*[56] recently demonstrated a sorting mechanism based on piezoelectrically actuated flow switching (Fig. 15). By integrating piezoelectric (PZT) actuators (response time of 0.1–1 ms) on-chip using a UV-ozone based bonding methodology, the authors can switch fluid flow to achieve a high throughput (>1000 cells/s) using a low applied voltage (<10 $V_{\text{p-p}}$).

To further the study, Cho *et al.*[61] recently incorporated the optofluidic waveguide technology into the chip to achieve high-efficiency illumination by guiding light inside the Teflon AF coated microfluidic channel. The method enables detection at multiple locations along the fluidic channel. In addition, the authors have designed a spatial filter, complemented with a low timing-jitter electronics system (field-programmable gate array-based) with preprogrammed real-time signal processing algorithms [Figs. 16(a)–16(c)], to perform high-speed, real-time sorting.

The system architecture described above [illumination, spatial filter, and digital signal processing (DSP) algorithms] offers several unique advantages over other μFACS systems, including fast and low powered sorting, real-time signal amplification, and sorting event verification. As shown in Fig. 16(b), as a fluorescent particle passes the detection region, the encoded signal detected by the PMT would result in a three-lobed signal (i.e., 111). By using a finite impulse response filter, the real-time DSP can amplify the detected signal by ~ 18 dB.[56] Once the amplified signal reaches the user-defined threshold, the system generates an output voltage waveform (after a set time delay) to trigger PZT actuation for sorting. Once the targeted particle is sorted to the right or left channel, the encoded signals from the spatial filter would register as 1101 or 1011, informing the user of the success of a sorting event, as illustrated in Fig. 16(d). On the other hand,

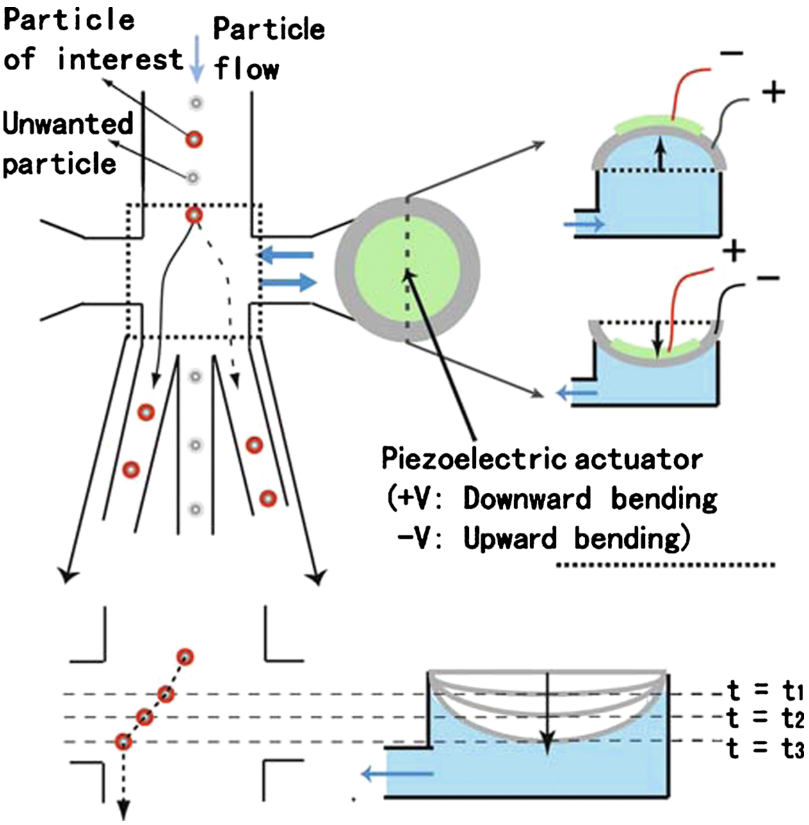

FIG. 15. Sorting mechanism of the piezoelectric (PZT)-actuated cell sorter. The voltage-induced PZT bending causes temporary fluid displacement (to the right or left), leading to deflection of targeted particles down to either side of the collection channels. The polarity and magnitude of the input voltage control the direction and magnitude of the deflection, respectively. Without PZT actuation, nontargeted cells exit directly down the waste channel (Ref. 56).

the absence of the verification signal signifies an unsuccessful sorting attempt. The capability to verify each sorting event in real time allows users to optimize the sorting conditions (i.e., sample flow rate, timing delay, actuator driving voltage, threshold setting, etc.) during the experiment. With this integrated μFACS architecture, the sorting of beads, mammalian cells[61] (Fig. 17), and fluorescence *in situ* hybridization (FISH)-labeled *E. coli*.[76] at a throughput of >1000 cells/s and an enrichment factor of >200 (highest among μFACS systems) has been demonstrated.

Although the MoFlo (a high-end commercial FACS) still outperforms the integrated μFACS under similar sorting conditions (achieving 920-fold enrichment factor at 2000 particles/s),[61] the much greater complexity, size, and the cost of the MoFlo ($\sim$\$500k) must be taken into consideration. The current PZT-integrated μFACS still lacks three-dimensional (3D) focusing as well as light scattering detection capabilities, which are two main factors contributing to the performance gap. By integrating a 3D flow module, such as the chevron structures demonstrated by the Ligler group,[42] velocity variations in the z-direction could be minimized, enhancing the sorting efficiency and reducing sorting errors. Moreover, the forward scattering (FSC) parameter can be readily incorporated by integrating on-chip waveguides and/or lens structures[46,47] that allow in-plane optical excitation and collection. With the FSC information, control algorithms can be implemented to abort the sorting of cells that travel too close to each other to avoid the “coincidental errors.” These developments could lead to a truly handheld lab-on-a-chip cell sorting device at a cost of 10–100 times lower than the commercial FACS, making the technology affordable to individual clinics, hospitals, and research laboratories.

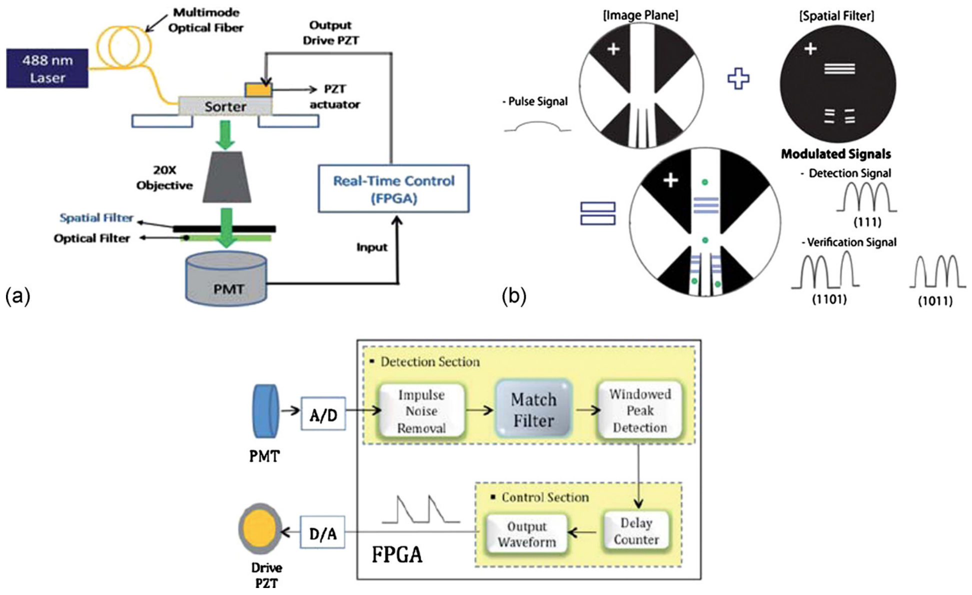
Multimode Optical Fiber
488 nm Laser
Output Drive PZT
Sorter
PZT actuator
20X Objective
Spatial Filter
Optical Filter
Real-Time Control (FPGA)
Input
PMT
(a)
[Image Plane]
[Spatial Filter]
- Pulse Signal
Modulated Signals
- Detection Signal
(111)
- Verification Signal
(1101)
(1011)
(b)
Detection Section
Impulse Noise Removal
Match Filter
Windowed Peak Detection
A/D
PMT
Control Section
Delay Counter
Output Waveform
D/A
FPGA
Drive PZT

FIG. 16. Schematics showing the external and internal workings of the integrated μFACS system. (a) Schematics of the setup showing on-chip illumination, spatial filter (transparency mask) modulated fluorescent detection, and FPGA-embedded electronic control system. (b) The spatial filter is placed at the image plane of the device, resulting in modulated fluorescence signals detected by the PMT when a fluorescent cell passes the detection zone (producing a 111 signal) and the postsorting region (producing a 1101 or 1011 signal, depending on the collection channel). (c) The FPGA-implemented real-time process control unit enables real-time signal amplification (~18 dB Signal to Noise Ratio enhancement) of the modulated signals by using a match filter. The control unit outputs a time-delayed waveform (user-defined) to trigger PZT actuation when the detected signals reach the user-defined threshold. (d) An example of space-time coded signal by the spatial filter of (b). The 111 coded signal at the detection zone is followed by the 1011 coded signal, confirming a successful sorting event (Ref. 61).

V. CONCLUSION

Microfluidic flow cytometers offer the benefits of significant size and cost reduction as well as reductions in required sample and reagent volumes. In addition, microfluidic platforms offer the integration of functional components such as sample pretreatment (e.g., cell lysing or staining) and postsort cell culturing to create a micrototal analysis system on a chip (μTAS). Disposable chips further provide a sterile testing environment, reducing the chance of cross-contamination and the risks of handling biohazardous samples. Such a closed, integrated testing platform will provide

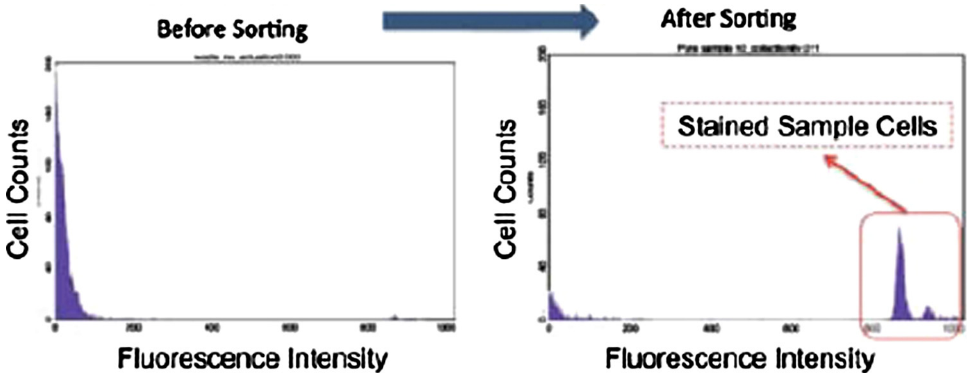

FIG. 17. Purity analysis of mammalian cell sorting. Before sorting (left histogram), the initial mixture ratio of nonfluorescent to fluorescent cells is ~1:150. After sorting by the μFACS, the final mixture ratio is ~1.86:1 showing an enrichment factor of 230-fold (Ref. 61).

further time and cost savings for researchers and clinicians, ultimately opening new doors for biomedical research. The development of a microfluidic flow cytometer may be the advance that brings a cytometer to every research laboratory, expediting discovery and understanding in areas such as cancer research, drug development, and genetics. Low-cost portable devices could allow HIV monitoring in remote areas of Africa and Asia, helping antiretroviral drugs make their way to patients in need. Low-cost microfluidic devices could further help patients in affluent countries to receive faster test results, and may reduce the amount of blood required for testing.

There are, however, a number of important obstacles to overcome in order for microfluidic flow cytometers to rival and eventually replace current benchtop flow cytometers. Microfluidic systems, first of all, should be able to deliver all cells (regardless of polarizability, size, etc.) along the microfluidic channel at a uniform speed regardless of the flow rate to prevent "coincidence events" at the interrogation zone and false-sorting at the sorting junction. Integrated optical detection systems must demonstrate their ability to truly rival the sensitivity and resolution of benchtop flow cytometers. To date, considerable progress has been made toward achieving these critical benchmarks, but there is work remaining to be done. In addition, selecting the right material and developing proper mass-fabrication techniques are essential to lowering the cost of the microfluidic flow cytometer. Further, while a miniaturized optofluidic cytometry chip addressing each of these issues may sound like a total solution, the size of the whole system must still be addressed. Components such as the lasers, detectors, fluidic pumps, actuators, and electronics can make the final chip-interfacing system considerably larger, in turn making the entire ensemble less attractive for practical on-the-spot testing or point-of-care applications. Many researchers are working to resolve these issues, resulting in the novel approaches discussed in this work.

Fluid focusing using inertial effects in fluidic channels may enable reliable three-dimensional fluid focusing without the use of additional fluidic pumps, enhancing the quality of signals and reducing the size of the fluidic system. Newly demonstrated multicolor detection technology invented by the Lo group, known as COST coding, holds great promise for compactness by fundamentally altering the scaling rule (i.e., the number of required optical components will no longer scale linearly with the number of detection parameters). Optofluidic waveguides can be used to enhance the coupling efficiency of photons to samples, thus increasing sensitivity and permitting multispot illumination. Lastly, the demonstration of fast-response deflectors (e.g., PZT actuators) in conjunction with a high-speed, low jitter closed loop control systems shows potential for microfluidic sorters to greatly exceed the demonstrated 1000 cells/s, holding promise to rapidly move into the realm of being competitive with benchtop sorters.

Upon satisfying these stringent yet quite achievable requirements, the field of optofluidics holds great promise for flow cytometry, offering the development of a low-cost, compact portable flow cytometer and FACS system that can be readily afforded by individual clinics and research laboratories. More importantly, such an emerging technology could provide point-of-care diagnosis and analysis in remote areas of Africa and Asia that continue to struggle with widespread epidemics, such as malaria and HIV. In short, the development of the compact, low-cost microfluidic flow cytometer promises to improve global quality of life; and although the technology is not fully ready today, great strides have been made (and continue to be made) toward achieving this goal.

ACKNOWLEDGMENTS

The authors acknowledged the excellent device fabrication infrastructure and the staff supports of the UCSD Nano3 Facility. We also thanked Dr. Kenichi Yamashita of AIST, Japan for his insight and fluidic dynamic simulations of microfluidic 3D flow confinement systems. The work was supported by the NIH (Grant Nos. R21RR024453 and R01HG004876).

[1] A. Givan, *Flow Cytometry: First Principles* (John Wiley & Sons, New York, 2001).
[2] H. Shapiro and R. Leif, *Practical Flow Cytometry* (Wiley-Liss, New York, 2003).
[3] A. Lehmann, S. Sørnes, and A. Halstensen, J. Immunol. Methods **243**, 229 (2000).
[4] R. Nunez, Current Issues in Molecular Biology **3**, 67 (2001).
[5] P. Pala, T. Hussell, and P. Openshaw, J. Immunol. Methods **243**, 107 (2000).

[6] M. Roederer, J. Brenchley, M. Betts, and S. De Rosa, Clinical Immunology **110**, 199 (2004).
[7] C. Jennings and K. Foon, Cancer Invest **15**, 384 (1997).
[8] J. Gratama, A. Orfao, D. Barnett, B. Brando, A. Huber, G. Janossy, H. Johnsen, M. Keeney, G. Marti, and F. Preijers, Cytometry **34**, 128 (1998).
[9] A. Hawkins and H. Schmidt, *Handbook of Optofluidics* (CRC, Boca Raton, FL, 2010).
[10] P. Chattopadhyay, D. Price, T. Harper, M. Betts, J. Yu, E. Gostick, S. Perfetto, P. Goepfert, R. Koup, and S. De Rosa, Nat. Med. **12**, 972 (2006).
[11] S. De Rosa, L. Herzenberg, and M. Roederer, Nat. Med. **7**, 245 (2001).
[12] J. Godin, C. Chen, S. Cho, W. Qiao, F. Tsai, and Y. Lo, Journal of Biophotonics **1**, 355 (2008).
[13] D. Ateya, J. Erickson, P. Howell, L. Hilliard, J. Golden, and F. Ligler, Anal. Bioanal. Chem. **391**, 1485 (2008).
[14] R. Dickover, S. Herman, K. Saddiq, D. Wafer, M. Dillon, and Y. Bryson, J. Clin. Microbiol. **36**, 1070 (1998).
[15] M. Keeney, I. Chin-Yee, R. Nayar, and D. Sutherland, J. Hematother **8**, 327 (1999).
[16] O. Reynolds, Philos. Trans. R. Soc. London **174**, 935 (1883).
[17] C. Chang, Z. Huang, and R. Yang, J. Micromech. Microeng. **17**, 1479 (2007).
[18] D. Huh, Y. Tung, H. Wei, J. Grotberg, S. Skerlos, K. Kurabayashi, and S. Takayama, Biomed. Microdevices **4**, 141 (2002).
[19] H. Klank, G. Goranovi, J. Kutter, H. Gjelstrup, J. Michelsen, and C. Westergaard, J. Micromech. Microeng. **12**, 862 (2002).
[20] J. Knight, A. Vishwanath, J. Brody, and R. Austin, Phys. Rev. Lett. **80**, 3863 (1998).
[21] C. Simonnet and A. Groisman, Appl. Phys. Lett. **87**, 114104 (2005).
[22] T. Stiles, R. Fallon, T. Vestad, J. Oakey, D. Marr, J. Squier, and R. Jimenez, Microfluid. Nanofluid. **1**, 280 (2005).
[23] N. Sundararajan, M. Pio, L. Lee, and A. Berlin, J. Microelectromech. Syst. **13**, 559 (2004).
[24] A. Wolff, I. Perch-Nielsen, U. Larsen, P. Friis, G. Goranovic, C. Poulsen, J. Kutter, and P. Telleman, Lab Chip **3**, 22 (2003).
[25] R. Yang, D. Feeback, and W. Wang, Sens. Actuators, A **118**, 259 (2005).
[26] P. Howell, Jr., J. Golden, L. Hilliard, J. Erickson, D. Mott, and F. Ligler, Lab Chip **8**, 1097 (2008).
[27] M. Lee, S. Choi, and J. Park, Lab Chip **9**, 3155 (2009).
[28] D. Di Carlo, Lab Chip **9**, 3038 (2009).
[29] S. Hur, H. Tse, and D. Carlo, Lab Chip **10**, 274 (2010).
[30] J. Park, S. Song, and H. Jung, Lab Chip **9**, 939 (2009).
[31] A. Sudarsan and V. Ugaz (unpublished).
[32] X. Mao, S. Lin, C. Dong, and T. Huang, Lab Chip **9**, 1583 (2009).
[33] J. Oakey, R. Applegate, Jr., E. Arellano, D. Carlo, S. Graves, and M. Toner, Anal. Chem. **82**, 3862 (2010).
[34] H. Steen, Cytometry **11**, 223 (1990).
[35] C. Bliss, J. McMullin, and C. Backhouse, Lab Chip **7**, 1280 (2007).
[36] M. Chabinyc, D. Chiu, J. McDonald, A. Stroock, J. Christian, A. Karger, and G. Whitesides, Anal. Chem. **73**, 4491 (2001).
[37] J. Godin and Y. Lo (unpublished).
[38] A. Kummrow, J. Theisen, M. Frankowski, A. Tuchscheerer, H. Yildirim, K. Brattke, M. Schmidt, and J. Neukammer, Lab Chip **9**, 972 (2009).
[39] K. Ro, K. Lim, B. Shim, and J. Hahn, Anal. Chem. **77**, 5160 (2005).
[40] S. Camou, H. Fujita, and T. Fujii, Lab Chip **3**, 40 (2003).
[41] S. Demming, A. Llobera, R. Wilke, and S. Büttgenbach, Sens. Actuators B **139**, 166 (2009).
[42] J. Golden, J. Kim, J. Erickson, L. Hilliard, P. Howell, G. Anderson, M. Nasir, and F. Ligler, Lab Chip **9**, 1942 (2009).
[43] J. Lim, S. Kim, J. Choi, and S. Yang, Lab Chip **8**, 1580 (2008).
[44] K. Mogensen, J. El-Ali, A. Wolff, and J. Kutter, Appl. Opt. **42**, 4072 (2003).
[45] Z. Wang, J. El-Ali, M. Engelund, T. Gotsaed, I. Perch-Nielsen, K. Mogensen, D. Snakenborg, J. Kutter, and A. Wolff, Lab Chip **4**, 372 (2004).
[46] J. Godin, V. Lien, and Y. Lo, Appl. Phys. Lett. **89**, 061106 (2006).
[47] V. Lien, Y. Berdichevsky, and Y. Lo, IEEE Photonics Technol. Lett. **16**, 1525 (2004).
[48] Q. Kou, I. Yesilyurt, V. Studer, M. Belotti, E. Cambril, and Y. Chen, Microelectron. Eng. **73–74**, 876 (2004).
[49] H. Chen and Y. Wang, Microfluid. Nanofluid. **6**, 529 (2009).
[50] N. Pamme, R. Koyama, and A. Manz, Lab Chip **3**, 187 (2003).
[51] J. Seo and L. Lee, Sens. Actuators B **99**, 615 (2004).
[52] J. Godin and Y. Lo, XXV Congress of the International Society for Advancement of Cytometry, 2010, p. 228.
[53] J. Lee, W. Choi, K. Lee, and J. Yoon, J. Micromech. Microeng. **18**, 125015 (2008).
[54] J. Godin and Y. Lo, Conference on Lasers and Electro-Optics, 2009 and 2009 Conference on Quantum Electronics and Laser Science Conference, CLEO/QELS 2009, 2009, pp. 1–2.
[55] J. Seo and L. Lee, *12th International Conference on Transducers, Solid-State Sensors, Actuators and Microsystems* (IEEE, New York, 2003), Vol. 2, pp. 1136–1139.
[56] C. Chen, S. Cho, F. Tsai, A. Erten, and Y. Lo, Biomed. Microdevices **11**, 1223 (2009).
[57] S. Tang, C. Stan, and G. Whitesides, Lab Chip **8**, 395 (2008).
[58] S. Cho, J. Godin, C. Chen, F. Tsai, and Y. Lo, Proc. SPIE **7135**, 71350M (2008).
[59] D. Wolfe, R. Conroy, P. Garstecki, B. Mayers, M. Fischbach, K. Paul, M. Prentiss, and G. Whitesides, Proc. Natl. Acad. Sci. U.S.A. **101**, 12434 (2004).
[60] S. Cho, J. Godin, and Y. Lo, IEEE Photonics Technol. Lett. **21**, 1057 (2009).
[61] S. Cho, C. Chen, F. Tsai, J. Godin, and Y. Lo, Lab Chip **10**, 1567 (2010).
[62] S. Cho, W. Qiao, F. Tsai, K. Yamashita, and Y. Lo, Appl. Phys. Lett. **97**, 093704 (2010).
[63] J. Godin and Y. Lo (unpublished).
[64] N. Baumgarth and M. Roederer, J. Immunol. Methods **243**, 77 (2000).
[65] M. Land and D. Nilsson, *Animal Eyes* (Oxford University Press, New York, 2002).

[66] J. Ferrell, Jr. and E. Machleder, Science **280**, 895 (1998).
[67] T. Huang, T. Chu, H. Chen, and C. Jen, FASEB J. **14**, 797 (2000).
[68] J. Marcus, W. Anderson, and S. Quake, Anal. Chem. **78**, 956 (2006).
[69] M. Teruel and T. Meyer, Science **295**, 1910 (2002).
[70] P. Dittrich and P. Schwille, Anal. Chem. **75**, 5767 (2003).
[71] A. Y. Fu, C. Spence, A. Scherer, F. Arnold, and S. Quake, Nat. Biotechnol. **17**, 1109 (1999).
[72] D. Holmes, M. Sandison, N. Green, and H. Morgan, Proceedings of MicroTAS2004, 2004, Vol. 1, pp. 6–8.
[73] M. Wang, E. Tu, D. Raymond, J. Yang, H. Zhang, N. Hagen, B. Dees, E. Mercer, A. Forster, and I. Kariv, Nat. Biotechnol. **23**, 83 (2005).
[74] A. Fu, H. Chou, C. Spence, F. Arnold, and S. Quake, Anal. Chem. **74**, 2451 (2002).
[75] J. Krüger, K. Singh, A. O'Neill, C. Jackson, A. Morrison, and P. O'Brien, J. Micromech. Microeng. **12**, 486 (2002).
[76] C. Chen, S. Cho, S. Chiang, F. Tsai, Y. Lo, and K. Zhang (unpublished).
[77] N. Pamme and A. Manz, Anal. Chem. **76**, 7250 (2004).
[78] T. Laurell, F. Petersson, and A. Nilsson, Chem. Soc. Rev. **36**, 492 (2007).
[79] T. Chung and H. Kim, Electrophoresis **28**, 4511 (2007).
[80] D. Huh, W. Gu, Y. Kamotani, J. Grotberg, and S. Takayama, Physiol. Meas **26**, R73 (2005).
[81] N. Pamme, Lab Chip **7**, 1644 (2007).
[82] L. Fu, R. Yang, C. Lin, Y. Pan, and G. Lee, Anal. Chim. Acta **507**, 163 (2004).
[83] S. Fiedler, R. Hagedorn, T. Schnelle, E. Richter, B. Wagner, and G. Fuhr, Anal. Chem. **67**, 820 (1995).
[84] J. Voldman, M. Gray, M. Toner, and M. Schmidt, Anal. Chem. **74**, 3984 (2002).
[85] A. Ashkin and J. Dziedzic, Science **235**, 1517 (1987).
[86] A. Ashkin, J. Dziedzic, and T. Yamane, Nature (London) **330**, 608 (1987).